Desalination and Water Treatment
www.deswater.com

doi:10.5004/dwt.2018.22587

116 (2018) 137–147
June

Adsorption of Cu^{2+} from aqueous solutions by Si-substituted carbonate hydroxyapatite prepared from egg-shell: kinetics, isotherms and mechanism studies

Rongying Zeng[a,b], Wenqing Tang[b,*], Xing Liu[b], Chunxia Ding[a], Daoxin Gong[a,*]

[a]*College of Resources & Environment, Hunan Agricultural University, Changsha 410128, China, email: zengry13@163.com (R. Zeng), liuxing1127@sina.com (X. Liu), dcxxcn@163.com (C. Ding), gdx4910@163.com (D. Gong)*
[b]*College of Chemistry and Materials Science, Hengyang Normal University, Hengyang 421008, China, email: wqtang518@163.com (W. Tang)*

Received 29 September 2017; Accepted 5 June 2018

ABSTRACT

Si-substituted carbonate hydroxyapatite (Si-CHAP) was obtained by embedding silicate and carbonate into hydroxyapatite prepared from egg-shell via sonochemistry coprecipitation. Batch experiments were performed to investigate the effect of contact time, solution pH and temperature on the adsorption of Cu^{2+} by Si-CHAP. Our results showed that the maximal adsorption capacity, Q_m of Cu^{2+} reached to 246.80 mg g^{-1} at pH 5.7, and at 90 min contact time under 313 K. Adsorption kinetics followed pseudo-second order. The equilibrium process fit the Langmuir isotherm model and the maximum adsorption capacity of Si-CHAP for Cu^{2+} was found to be 273.51 mg g^{-1}. The thermodynamic studies showed that the adsorption of Si-CHAP on Cu^{2+} was a spontaneously endothermic process. Si-CHAP was characterized by using FTIR, XRD and SEM-EDS. The mechanism of Cu^{2+} adsorption by Si-CHAP may include ion exchange, precipitation and electrostatic interactions. Furthermore, the well stability properties of the Si-CHAP adsorbent were confirmed through desorption assays. These results showed that Si-CHAP has the potential to become a cheap and efficient adsorbent to remove Cu^{2+} from aqueous solutions.

Keywords: Adsorption; Si-substituted carbonate hydroxyapatite; Cu; Mechanism; Kinetics; Isotherms

1. Introduction

Copper (Cu) is an essential element to all living organisms (plants, animals, and humans) as it is a key constituent of some metalloenzymes and metalloproteins [1], and participates in the energy metabolism [2]. However, high concentration of Cu^{2+} can cause various diseases such as vomiting, diarrhea, hemolytic jaundice, kidney failure, nervous system damage and even cancer [3]. Thus, the maximum acceptable concentration of Cu^{2+} in drinking water were recommended at 2 mg L^{-1} by the World Health Organization (WHO) [4]. The recommendation of China regarding the safe amount of Cu^{2+} is 1 mg L^{-1} in drinking water (Standards for drinking water quality, GB 5749-2006). The US Environment Protection Agency (USEPA) sets the copper concentrations in industrially discharged wastewater at < 1 mg L^{-1} as a daily average (4.5 mg L^{-1} maximum daily) and state and local regulations further limit copper concentrations to between 10 and 100 ug L^{-1} (USEPA Regulation 40 CFR 413) [5(a)]. According to EU regulations, the maximum permissible concentrations (*MPC*) of copper is 0.5 mg L^{-1}. The standards of the Russian Federation generally imply that the *MPC* values is 0.1 mg L^{-1} for copper [5(b)].

However, the preparation or usage of Cu, including metallurgy, electroplating, dyeing, pigments and antimicrobial, inevitably generate wastewater containing high concentrations Cu^{2+}. To remove the hazardous effect of Cu^{2+} on ecosystem and public health from wastewaters, various

*Corresponding author.

treatment methods and technologies were reported, including chemical oxidation or reduction [6], chemical precipitation [7], membrane separation [8], ion exchange [9] and adsorption [10]. Among these methods, adsorption is one of the most effective, practical and economical methods for removing the heavy metals owing to its low cost, high adsorption efficiency, simple design and strong operability for metal ions [10]. Recently, various environment-friendly sorption materials such as chitosan [11], agricultural wastes [12], vermiculites [13], birnessite [14], and activated carbon [15] have been regarded as good new synthetic compounds.

Hydroxyapatite (HAP) has recently been found to be an environment-friendly adsorbent due to its particular crystal-chemical structure [16]. Previous studies have shown HAP can remove heavy metal ions like Cu, Zn, Cd and Pb ions from aqueous solutions [17,18]. To enhance the adsorption capacity of HAP, carbonate-substitution was investigated and the obtained carbonate-substituted hydroxyapatite (CHAP) was reported to have higher efficiency in the removal of heavy metals than HAP [19]. Moreover, we investigated the effect of Ca/P molar ratios on the adsorption of Cr(VI) by nano-CHAP and have found the adsorption capacity enhances with the increase of Ca/P molar ratio [20]. On the other hand, recent research shows that the surface area of HAP can be enhanced by adding of $SiO_4$4-substitutions [21]. However, the adsorption behavior of heavy metals on Si-substituted carbonate hydroxyapatite (Si-CHAP) is largely unknown.

The effect of some parameters such as contact time, solution pH and temperature on the adsorption of Cu^{2+} by Si-CHAP was studied. Furthermore, desorption assays were performed to study the stability properties of the Si-CHAP. The underlying mechanisms on copper sorption by Si-CHAP were investigated by using scanning electron microscopy coupled with energy dispersive spectrometer (SEM-EDS), X-ray diffraction (XRD).

2. Materials and methods

2.1. Si-CHAP preparation

Si-CHAP was prepared by sonochemical co-precipitation, a method as described previously [20,22]. In brief, eggshells (from Hengyang Normal University Canteen) were rinsed three times with de-ionized water, and dried in the oven at 353 K. Then, the treated egg-shells were ground and sieved into powder (mesh size is 30).

With continuous ultrasound application, eggshell powder was vigorously added to H_3PO_4 (purity >85%, Hunan, China) in a molar ratio 1:1. The temperature, pH value and reaction time were kept at 303–313K, 3–4 and 2–3 h, respectively. The reaction taken place according to the following Eq. (1):

$$CaCO_3 + H_3PO_4 = CaHPO_4 + CO_2\uparrow + H_2O \quad (1)$$

Then $Ca(OH)_2$ was added into the above mixtures with keeping the temperature at 323–333K and pH 10.5–11.5 (adjusting pH by ammonia). Finally, highly dispersed and gel-like nascent Hydroxyapatite (HAP) product was obtained. Introduction of Na_2SiO_3 and Na_2CO_3 into the nascent HAP product with concurrent use of continuous ultrasound could effectively result in group substitution of HAP by CO_3^{2-} and SiO_4^{4-}. The reactions were described by the following chemical Eq. (2):

$$CaHPO_4 + Na_2CO_3 + Na_2SiO_3 + Ca(OH)_2 \rightarrow Ca_{10}(PO_4)_{6-x-y}(SiO_4)_x(CO_3)_y(OH)_{2-x+y} \quad (2)$$

The resulted suspension was collected, dried and ground into powder (mesh size is 30), namely Si-CHAP.

2.2. Characterization of Si-CHAP

To study the crystallinity of the prepared Si-CHAP, powder X-ray diffraction (XRD, Rigaku MiniFlex X-ray diffractometer, Japan) patterns were recorded. Fourier transform infrared spectroscopic (FT-IR-8700, Shimadzu Corporation, Japan) analysis was performed to identify the presence of chemical functional groups in the Si-CHAP. Scanning electron microscopy (SEM, HitachiJSM-5600LV) was conducted to observe the surface microstructures. Energy dispersive spectrometer (EDS:IE 300 X) was used for the elemental analysis of the adsorbent.

2.3. Adsorption studies

All chemicals used were of analytical reagent grade. The stock solution containing 1000.00±1 mg L^{-1} Cu^{2+} was prepared by using $Cu(NO_3)_2$ with de-ionized distilled water. Adsorption equilibrium assays were carried out by adding 0.60 g L^{-1} Si-CHAP in 100 mL of Cu^{2+} solution at the desired concentration in a thermostatic shaker with a constant agitation speed of 150 rpm. To investigate the adsorption isotherm, the contact time was varied from 15 min to 150 min at temperatures of 293, 303 and 313K, respectively. The effects of initial solution pH on the removal efficiency were investigated. The pH was adjusted from 1.5 to 7.5 by NaOH and HNO_3 (dosage of 0.06 mg, contact time for 90 min, temperature at 303K). When the equilibrium was reached, the suspensions were filtrated, and the Cu^{2+} concentration in the filtrate was determined by the flame atomic absorption spectrophotometer (FAAS) (PE700, PE Company, USA).

The amount Q_e and Q_t of the Cu^{2+} adsorbed onto Si-CHAP were calculated by a mass balance relationship using the following equations: Eq. (3) and Eq. (4):

$$Q_e = (C_0 - C_e)V/m \quad (3)$$

$$Q_t = (C_0 - C_t)V/m \quad (4)$$

where Q_e (mg g^{-1}) is the equilibrium adsorption capacity; Q_t (mg g^{-1}) was the adsorption capacity at time t; C_0 and C_e are the initial and equilibrium concentration(mg L^{-1}) of Cu^{2+} in solution; C_t is the concentration of Cu^{2+} at time t (mg L^{-1}); V (L) is the volume; and m (g) is the weight of the adsorbent.

2.4. Kinetic study

To better understand the adsorption process, pseudo-first-order, pseudo-second-order and intraparticle dif-

fusion models were used to describe the equilibrium data for the Cu^{2+} adsorption on Si-CHAP. These models are commonly used to simulate the adsorption behavior of pollutants on solid surfaces [20,23,24]. The three models, equations can be written as Eqs. (5)–(7):

Pseudo-first-order equation: $$Q_t = Q_e(1 - \exp(-K_1 t)) \quad (5)$$

Pseudo-second-order equation: $$Q_t = (tK_2Q_e^2)/(1 + tK_2Q_e) \quad (6)$$

where K_1 (min^{-1}) and K_2 (g mg^{-1} min^{-1}) are the rate constants of first-order and second-order model, respectively.

Intraparticle diffusion can be estimated by using the Weber–Morris intraparticle diffusion model [18]:

$$Q_t = K_{id}\, t^{0.5} + C \quad (7)$$

where K_{id} (g mg^{-1} $min^{-0.5}$) is the intraparticle diffusion rate coefficient and C represents the boundary layer effect of adsorption.

2.5. Adsorption isotherms

Langmuir and Freundlich isotherm models have been widely used to describe adsorption data [23,24].

The Langmuir model assumes that maximum adsorption occurs at monolayer adsorption onto a surface, and there is no transmigration of adsorbate in the plane of the surface. The original form of Langmuir isotherm model is given [25]:

$$Q_e = Q_m K_{eq} C_e/(1 + K_{eq} C_e) \quad (8)$$

where Q_m and K_{eq} represent the maximum adsorption capacity (mg g^{-1}) and the affinity adsorption constant (L mg^{-1}). The essential characteristics of a Langmuir isotherm can be expressed using a dimensionless separation factor or an equilibrium parameter R_L, which is calculated by the following Eq. (9) [20]:

$$R_L = 1/(1 + K_{eq} C_0) \quad (9)$$

The R_L parameter is considered as a more reliable indicator of the adsorption. The R_L value may be interpreted for four shapes: (i) unfavorable adsorption ($R_L > 1$), (ii) linear adsorption ($R_L = 1$), (iii) favorable adsorption ($0 < R_L < 1$), (iv) irreversible adsorption ($R_L = 0$).

Freundlich isotherm is usually used to heterogeneous surface energy systems and based on the assumption that the adsorption sites are distributed exponentially. The equation is given by Eq. (10) [26]:

$$Q_e = K_f C_e n \quad (10)$$

where K_f is the Freundlich dissociation constant (mg g^{-1}) and n the Freundlich exponent. K_f and n constants depend on temperature and properties of adsorbate and adsorbent. They represent the adsorption capacity of adsorbent and adsorption intensity, respectively [23]. The values of n less than 1 represent a favorable adsorption [24].

2.6. Sorption thermodynamics

The adsorption thermodynamics parameters such as Gibbs energy change (ΔG^0), enthalpy change (ΔH^0), and entropy change (ΔS^0) were obtained using the following equations [27]:

$$\Delta G^0 = -RTlnK_{eq} \quad (11)$$

$$lnK_{eq} = \Delta S^0/R - \Delta H^0/(RT) \quad (12)$$

in which ΔG^0, ΔS^0, ΔH^0, R and T are gibbs free energy (J mol^{-1}), entropy change (J mol^{-1}), enthalpy change (J mol^{-1}), universal gas constant (8.314 J $(mol\ K)^{-1}$), and temperature (K), respectively.

3. Results and discussion

3.1. FTIR analysis

FTIR was employed to quantify the hydroxyl, carbonate, silicate and phosphate groups of the Si-CHAP, HAP and eggshell. As shown in Fig. 1, a band at 3425 cm^{-1} was obscured by a broad band between 3200 and 3650 cm^{-1}, which is assigned to the stretching mode of hydroxyl group [28]. A weak band at 2123.4 cm^{-1} can be assigned to surface P-OH stretching modes [29]. A band in the 1990.4 cm^{-1}, possibly due to surface adsorbed HPO_4^{2-} groups [28]. The bands at 1650 and 1458 cm^{-1} correspond to carbonate for the samples [30]. The typical absorption bands of the PO_4^{3-} group in Si-CHAP at 950^{-1} 120 cm^{-1}, 557 cm^{-1} and 621 cm^{-1} could be observed. The band appearing at 877 cm^{-1} is assigned to Si-O vibration modes, 796 cm^{-1} is assigned to Si-O-Si bending modes [31]. In the spectrum of HAP, typical absorption bands of the PO_4^{3-} group and hydroxyl group are similar with Si-CHAP. In the spectrum of eggshell, the most significant peak of intensity at 1417.6 cm^{-1}, strongly associated with the presence of carbonate minerals within the eggshell [32]. There is also one observable peak at about

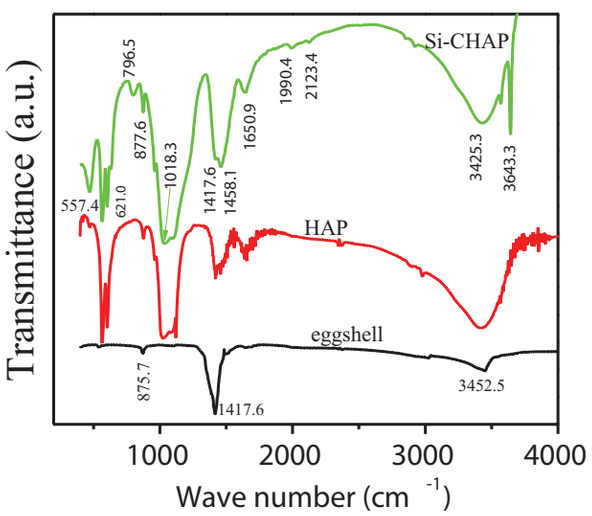

Fig. 1. FTIR spectra of Si-CHAP, HAP and eggshell.

875 cm^{-1}, which should be associated with out-plane deformation mode, in the presence of calcium carbonate [32].

3.2. Effect of contact time

The effect of contact time on the removal of Cu^{2+} by Si-CHAP at three temperatures (T = (293, 303 and 313) K) is shown in Fig. 2. Two stages could be included: in the first 30 min, the adsorption percentage increased rapidly; thereafter, the adsorption rate decreased gradually, and the adsorption reached an equilibrium at around 90 min. When the contact time came up to 150 min, the Cu^{2+} removal rate increased by about 1% from 90 min to 150 min at 293, 303 and 313 K (Fig. 2). The results could be explained by following: first, this rapid adsorption could be attributed to a larger surface area of the adsorbent being available for the adsorption of the metals; then, the adsorption continued at a slower rate and finally reached to the equilibrium due to the saturation of adsorption sites on adsorbent surface [33,34]. Thus, 90 min was chosen for our following experiments. Furthermore, the adsorption curves indicated the possible monolayer coverage on the adsorbent surface by Cu^{2+} because they were continuous, pseudo-smooth, single and leading to saturation.

3.3. Effect of the pH

The earlier studies have shown that solution pH is an important parameter influencing metal ions adsorption because it affected the charge state of the adsorbent surface and the species of adsorbate [20]. The effect of pH on adsorption of Cu^{2+} onto the Si-CHAP was investigated by varying the solution pH from 1 .5 to 7.5 (Fig. 3). The distribution coefficient of copper species in the solution pH range of 1.0–14.0 was determined by using Visual MINTEQ 3.0 (Fig. 4). The dominant species of copper are Cu^{2+}, $Cu_2(OH)_2^{2+}$, $Cu_3(OH)_4^{2+}$, $Cu(OH)_3^-$ and $Cu(OH)_4^{2-}$ at the different solution pH values. As shown in Fig. 3, at pH < 5.7, the adsorption capacity of Si-CHAP increased sharply along with the increase of the pH value. The reason is probably that, under strong acidic conditions, copper existed mainly in the form of Cu^{2+}, $Cu_2(OH)_2^{2+}$, $Cu_3(OH)_4^{2+}$ (Fig. 4), H^+ competed with them for adsorption sites; however, with the increase of pH value, the competition from H^+ decreased and Cu^{2+} could be adsorbed on the adsorbent quite easily. When the pH > 5.7, the removal efficiency decreased slightly as pH increased, possibly caused by the formation of soluble hydroxyl complexes. The optimal pH of 5.7 was chosen for the adsorption studies.

The point of zero charge (pH_{PZC}) is defined as the pH at which the total surface charges become zero as described previously [35]. The point of zero charge (pH_{PZC}) is an important parameter used to describe variable-charge surface of adsorbent. If the optimal pH > pH_{PZC}, adsorbent surface would have a net negative charge and predominantly exhibits an ability to adsorb cations; If the optimal pH < pH_{PZC}, adsor-

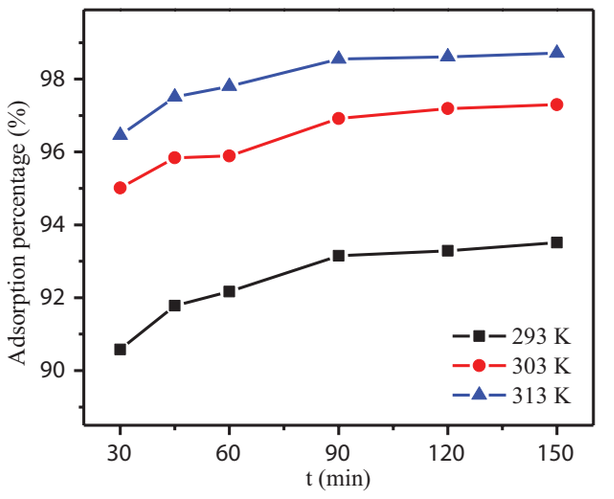

Fig. 2. Effect of contact time on the adsorption of Cu^{2+} by Si-CHAP (C_0 = 150 mg·L^{-1}, pH = 5.7, Si-CHAP dosage = 0.6 g·L^{-1}, t = 90 min).

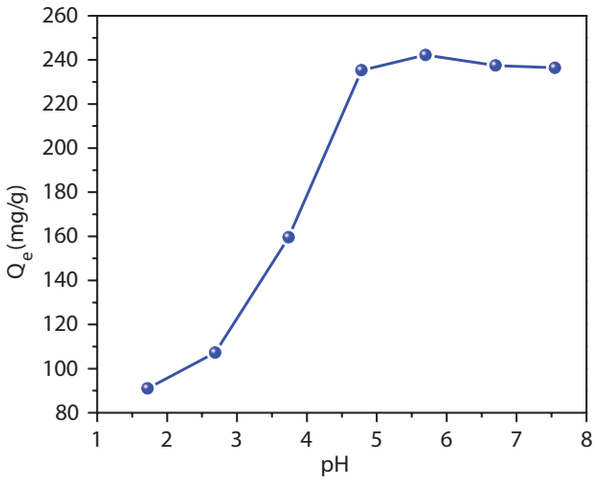

Fig. 3. Effect of pH on the Cu^{2+} sorption by Si-CHAP (C_0 = 150 mg·L^{-1}, Si-CHAP dosage = 0.6 g·L^{-1}, t = 90 min, T = 303K.).

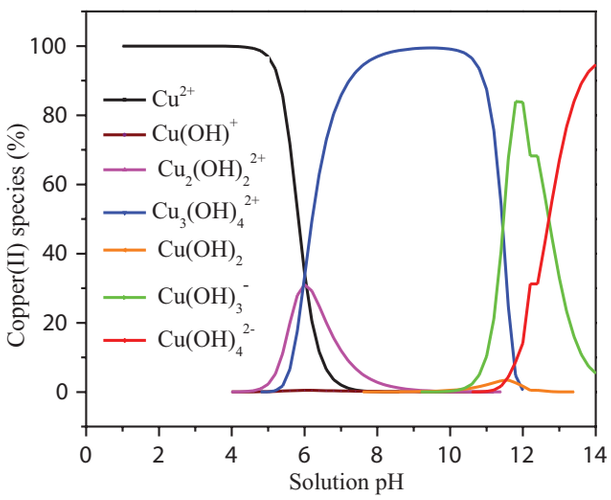

Fig. 4. Ratio of copper hydroxy complex ions to pH.

bent surface would have a positive charge and appeals to adsorb negative ion [36]. Thus, the experiments were carried out in ten Erlenmeyer flasks with stopper cork which containing 50 mL of 0.01 M $NaNO_3$ solution. The initial pH (pH_i) in the range of 1.0–10.0 was adjusted by 0.1 M NaOH or 0.1 M HNO_3 solutions in each Erlenmeyer flask. 0.2 g Si-CHAP was added to each flask, which were kept for 48 h with intermittent manual shaking to attain the equilibrium. The difference of the initial and final pH (pH_f) values ($\Delta pH = pH_i - pH_f$) was plotted against the pH_i. The point of intersection of the resulting curve with abscissa, at which $\Delta pH = 0$, showed the pHpzc. The observed pH_{PZC} for Si-CHAP was 4.42, which is less than the optimal pH 5.7. Therefore, the Si-CHAP surface is net negatively charged, which is favorable in complexing Cu^{2+} on the sorbent surface.

3.4. Kinetic studies

The kinetic parameters in Eqs. (5)–(7) could be derived from the fitted curves. The nonlinear curve plots of Q_t against t were fitted to determine the rate constants and correlation coefficients for the first, second-order kinetic models (Figs. 5a,b), respectively. The straight-line plots of Q_t against $t^{0.5}$ were used to determine the rate constants and correlation coefficients for intraparticle diffusion kinetic models (Fig. 5c). The kinetic parameters are listed in Table 1.

As seen in Table 1, at three temperatures, calculated adsorption values (Q_{cal}) of the first, second-order kinetic models showed a compliance with the experimental data (Q_{exp}). However, the maximum value of the correlation coefficient (R^2) of Cu^{2+} was 0.7333 in the pseudo-first-order model at 313K. The smallest value of correlation coefficients (R^2) was 0.9789 in the pseudo-second-order model at 293K. The correlation coefficients (R^2) for the intraparticle diffusion model were found to be 0.9023, 0.9300, 0.8249 at 293, 303, 313 K respectively. Thus, the kinetics of Cu^{2+} adsorption on the Si-CHAP closely followed the pseudo-second-order with higher correlation coefficient (R^2).

3.5. Adsorption isotherm

Fig. 6 shows the effect of initial Cu^{2+} ion concentration (C_0, 50–200 mg L^{-1}) and different temperature (293K, 303K, and 313K) on the adsorption capacity (Q_e) (mg g^{-1}). It is clear that the adsorption capacity increases with increasing initial Cu^{2+} ion concentration, as well as with the increase of temperature. This is most likely due to a greater availability of adsorbate ions in the vicinity of the adsorbent [18,37].

Next, Langmuir and Freundlich adsorption isotherms [Eqs. (8)–(10)] were used to analyze the experimental data at various temperatures (Langmuir and Freundlich adsorption isotherms were indicated by the solid lines in Figs. 7a and b, Experimental data were indicated by the dotted lines in Fig. 7a and their parameters are shown in Table 2. According to the shapes of the curves in Fig. 7a (dotted lines), the isotherms corresponding to Cu^{2+} adsorption may be classified as L-type of the Giles classification [38]. The L-type isotherm suggests a relatively high affinity between Cu^{2+} and Si-CHAP. This also indicates that no strong competition occurs for the adsorption sites between solvent molecules and adsorbate molecules.

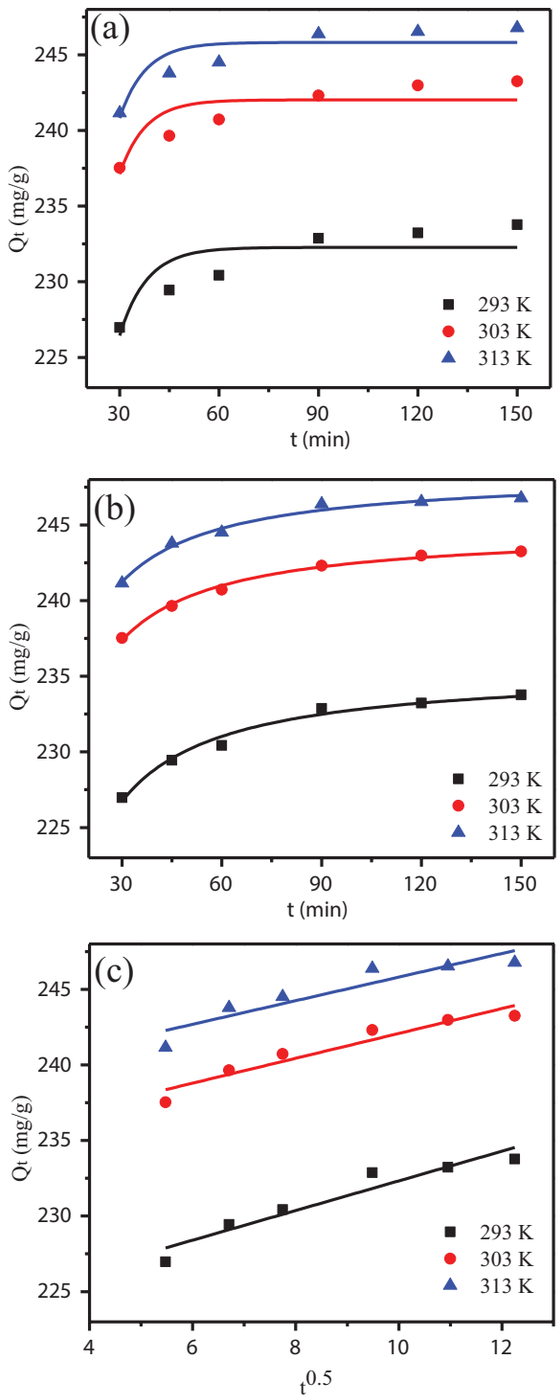

Fig. 5. Plots of pseudo-first-order kinetic equation (a), pseudo-second-order kinetic equation (b) and intraparticle diffusion equation (c). (C_0 = 150 mg·L^{-1}, pH = 5.7, Si-CHAP dosage = 0.6 g·L^{-1}).

From Table 2, the correlation coefficients (R^2) for the Langmuir model were (0.9538, 0.9554, and 0.9568), which were much higher than those of the Freundlich model (0.8927, 0.8891, 0.8428) at (293, 303, and 313) K, respectively. R_L value drops between 0 and 1 in all experimental systems,

Table 1
Kinetic model parameters for adsorption of Cu^{2+} onto Si-CHAP at different temperature

Kinetic models	Parameters	293K	303K	313K
Pseudo-first order	Q_{exp} (mg g^{-1})	234.375	243.451	246.800
	Q_{cal} (mg g^{-1})	232.271	242.020	245.818
	K_1 (min^{-1})	0.1228	0.1300	0.1298
	R^2	0.6317	0.6495	0.7333
Pseudo-second-order	Q_{cal} (mg g^{-1})	228.580	253.197	257.463
	K_2 (g (mg min)$^{-1}$)	0.9245	1.0054	1.1116
	R^2	0.9789	0.9932	0.9835
Intraparticle diffusion	K_{id} (mg $g^{-1}min^{-0.5}$)	0.9813	0.8227	0.7810
	C (mg g^{-1})	222.515	233.856	237.999
	R^2	0.9023	0.9300	0.8249

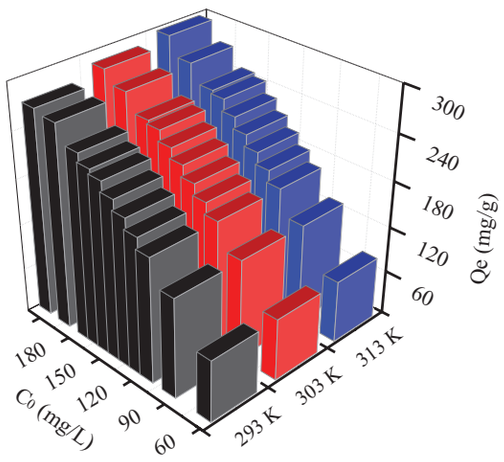

Fig. 6. Effect of initial Cu^{2+} ion concentration (C_0) and temperature on the adsorption capacity (Q_e) (mg g^{-1}). (pH = 5.7; t = 90 min; Si-CHAP dosage = 0.6 g/L).

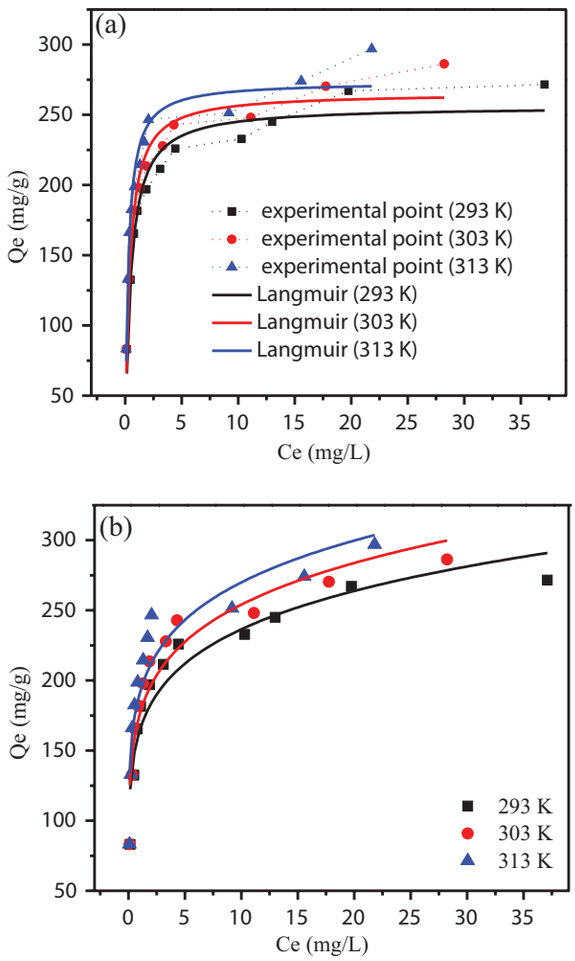

Fig. 7. Langmuir adsorption isotherm (a) and Freundlich adsorption isotherm (b). (pH = 5.7; t = 90 min; Si-CHAP dosage = 0.6 g/L).

which indicates favorable adsorption of the copper process. Lower R_L values at higher initial Cu^{2+} concentrations and temperature showed that adsorption was more favorable at higher concentration and appropriate temperature. Thus, the adsorption data could be best described by the Langmuir model, which suggesting porous Si-CHAP had a large of surface areas with monolayer adsorption sites for copper [39,40]. The maximum adsorption capacity (Q_m), and the adsorption constant (K_{eq}), were found to increase for an increase in the solution temperatures from 293 to 313K. The increase of the adsorption with the increase of temperature indicates that the adsorption is endothermic in nature [41]. According to Langmuir isotherm equation,the theoretical monolayer maximum uptake capacities (Q_m) of Si-CHAP is 273.52 mg g^{-1} at 313 K.

3.6. Thermodynamic studies

The linear plot of lnK_{ed} versus $1/T$ is shown in Fig. 8. Based on Eqs. (11)–(13), the calculated thermodynamic parameters for the adsorption of copper by Si-CHAP composite are given in Table 3. The negative Gibbs energy (ΔG^0) values of Cu^{2+} adsorption at various temperatures indicate the feasibility and spontaneous nature of the adsorption. Decreased ΔG^0 value with increasing temperature suggests that higher temperature contributes to the adsorption process. ΔH^0 and ΔS^0 of adsorption were 21.59 kJ mol^{-1} and 119.42 $J{\cdot}mol^{-1}{\cdot}K^{-1}$, respectively (Table 3). The positive value of ΔH^0 implies the endothermic nature of Cu^{2+} adsorption by Si-CHAP composite, which is supported by the increase in the adsorption capacity. The positive value of ΔS^0 suggests the freedom of Cu^{2+} ions during adsorption and the high degree of randomness at the solid-liquid during adsorption process [18,42].

3.7. Elution/adsorption and recycling studies

The reusability of Si-CHAP for Cu^{2+} adsorption was evaluated through many cycles of the adsorption/desorption. To this end, the Cu-adsorbed Si-CHAP sample (303K) was mixed with 100 ml of 0.1 M HNO_3 solution for 180 min

Table 2
Equilibrium model parameters for adsorption of Cu^{2+} onto Si-CHAP at different temperature

Equilibrium models	Parameters	293K	303K	313K
Langmuir isotherm	Q_m ($mg\ g^{-1}$)	256.104	265.631	273.515
	K_{eq} ($L\ g^{-1}$)	2.2319	2.7773	3.9385
	R^2	0.9538	0.9554	0.9568
	R_L	0.002–0.009	0.001–0.007	0.001–0.005
Freundlich isotherm	K_f ($mg\ g^{-1}$)	164.305	175.952	190.660
	$1/n$	0.1581	0.1595	0.1510
	R^2	0.8927	0.8891	0.8428

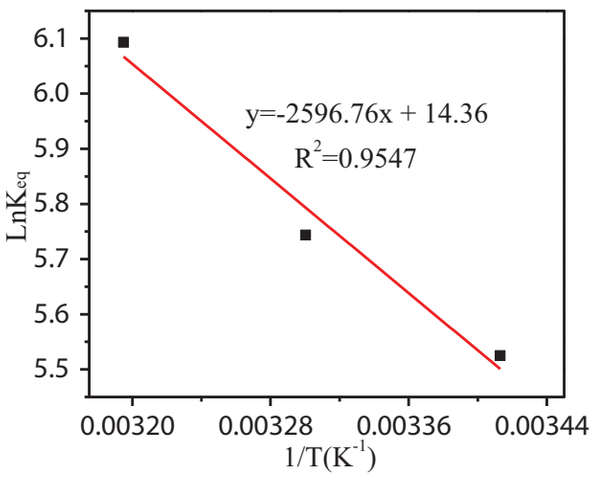

Fig. 8. Enthalpy determination curves for the sorption of copper ion onto Si-CHAP.

Table 3
Thermodynamic parameters for sorption of Cu^{2+} onto Si-CHAP

T (K)	ΔG^0(KJ·mol^{-1})	ΔH^0(KJ·mol^{-1})	ΔS^0(J·mol^{-1}·K^{-1})	R^2
293	–13.40	21.59	119.42	0.9547
303	–14.59			
313	–15.79			

at room temperature to remove the adsorbed Cu^{2+}. Then, the adsorption/desorption was recycled six times by the same procedure. It was found that the adsorption efficiency for Cu^{2+} by recycled Si-CHAP was 95.84%, 91.61%, 88.81%, 86.43%, 83.29% and 80.95%, corresponding to the six cycles, respectively. That the adsorption efficiency was reduced to 91.61% in cycle 2 and 88.81% in cycle 3 indicated partial pore structure might be collapsed during the recycling process. EDS image of the recycled Si-CHAP showed that the majority of the Cu^{2+} adsorbed by Si-CHAP have been removed by desorption methods (Fig. 9), indicating that ion exchange was one of the principle mechanism for the removal of Cu^{2+} and it was in accordance with the thermodynamic studies. Thus, this suggested that the Si-CHAP performed quite well for adsorption/elution Cu^{2+} from aqueous solution and may be feasible in its application on a large scale.

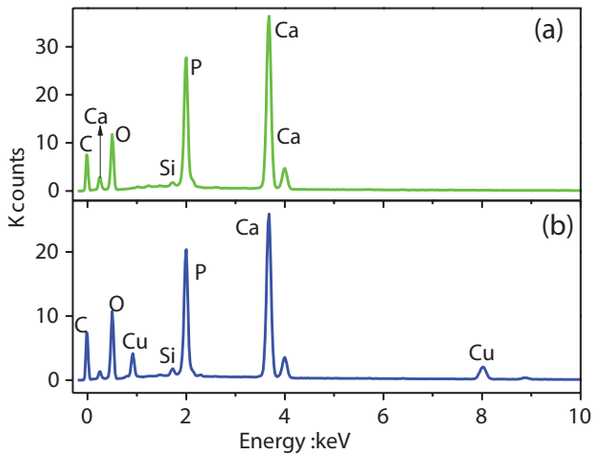

Fig. 9. EDS analysis of Si-CHAP during recycling: with (a) or without Cu^{2+} (b) desorption.

3.8. Mechanisms studies

Divalent cations removal by the ability of hydroxyapatite can be explained by two possible reaction mechanisms (ion-ion exchange and dissolution-precipitation) [43]. Mechanisms such as ion exchange, surface complexation, precipitation or substitution of Ca in hydroxyapatite by metal during recrystallization (coprecipitation) have been proposed previously [44]. Combined with the above studies, we speculated that the adsorption of Cu^{2+} by Si-CHAP may involve in three possible mechanisms.

The first possible mechanism is ion exchange reaction between Cu^{2+} adsorbed and Ca^{2+} of Si-CHAP. XRD patterns of Si-CHAP showed that after adsorption of Cu^{2+}, the positions of peaks were similar to that of before adsorption, but there was a decrease in the intensity and an increase in the width at around $2\theta = 32°$(Fig. 10). Lin et al. also suggested the crystal structure may lead to the abnormal shift of the diffraction peak position and the diffraction peak intensity change [45]. The ion exchange interactions can be presented as follows [46]:

$$Ca_{10}(PO_4)_{6-x-y}(SiO_4)_x(CO_3)_y(OH)_{2-x+y} + mCu^{2+} \rightarrow Cu_mCa_{10-m}(PO_4)_{6-x-y}(SiO_4)_x(CO_3)_y(OH)_{2-x+y} + mCa^{2+} \quad (13)$$

The second possible mechanism is surface complexation and electrostatic sorption. The solution pH has a significant

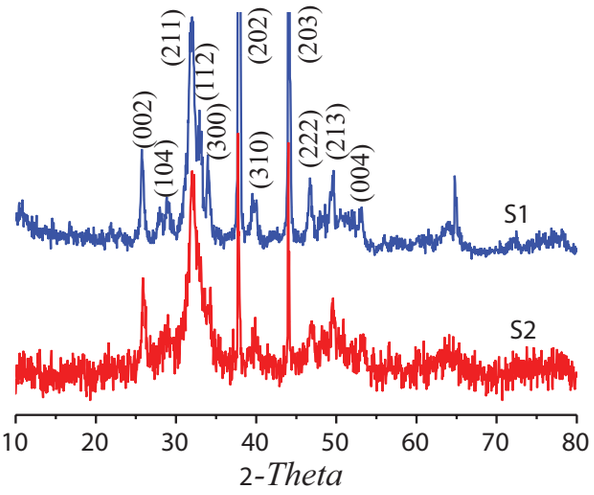

Fig. 10. XRD patterns of Si-CHAP (S1) and after adsorption of Cu^{2+} (S2).

effect on the surface charge of the adsorbent. Reactions involved in the surface reactions of Si-CHAP that relate to pH variation can be listed as follows [19]:

$$Ca\text{-}OH^{2+} \leftrightarrow Ca\text{-}OH^{0} + H+$$
$$P\text{-}O- + H+ \leftrightarrow P\text{-}OH^{0}$$

At lower pH (pH < pH_{PZC}, pH_{PZC} = 4.42), $Ca\text{-}OH^{2+}$ and neutral $P\text{-}OH^{0}$ would be the dominant elements at Si-CHAP surfaces. As a result, the surface of the sorbent is net positively charged. Increased net positive charge is less favorable in complexing Cu^{2+} on the sorbent surface than the net negative charge sites. Thus, increased net positive charge of the Si-CHAP surface in the pH range of 1.7–3.7 may be the cause of reduced Cu^{2+} removal (Fig. 3). P-OH surface groups (at 2123.4 cm^{-1} from IR in Fig. 1) from the protonation of surface PO_4^{3-} groups may form acidic phosphate ions (HPO_4^{2-} and $H_2PO_4^{-}$) to maintain surface charge balance. Since surface P-OH groups have been identified as an adsorption site [47], it is reasonable to deduce that they could serve as the predominant adsorption site for Cu^{2+}. Therefore, the surface complexation reaction can contribute to a removal of copper by the following general reactions:

$$P\text{-}OH + Cu^{2+} \rightarrow P\text{-}O\text{-}Cu^{+} + H^{+}$$

when pH close to or higher than the pH_{PZC}, the dominant surface elements are P-O- and $Ca\text{-}OH^{0}$. Thus, Cu^{2+} is adsorbed on the surface of Si-CHAP by the electrostatic attraction at the beginning of the adsorption behavior, which is coincidence with the reported elsewhere [48].

Finally, the surface precipitation and co-precipitation mechanism. As seen from the SEM in Fig. 11, the surface of Si-CHAP is rough and has lots of ravines and gullies, which suggests that Si-CHAP has a large of adsorption surface area. Compared with the SEM before adsorbing Cu^{2+} (Fig. 11a), the SEM after adsorption showed that

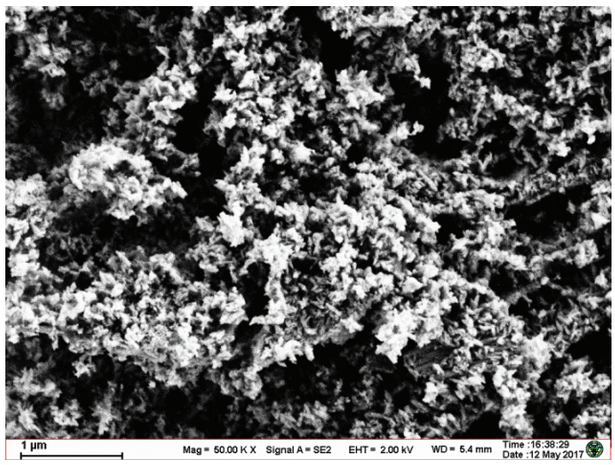

(a)

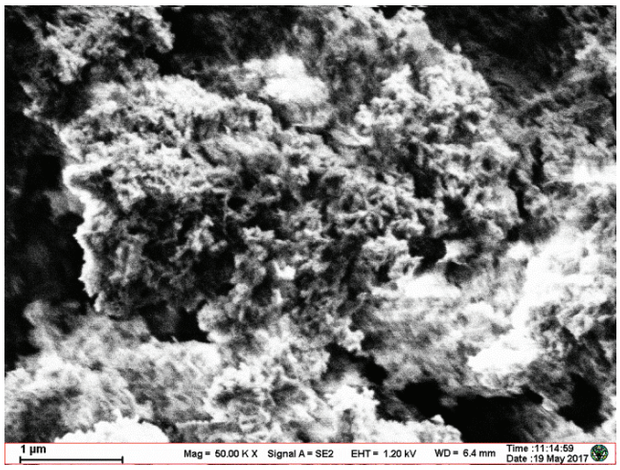

(b)

Fig. 11. SEM of before the adsorption (a)and (b)adsorption equilibrium on the Si-CHAP.

the adsorption of Cu^{2+} mainly appeared at the surface (Fig. 11b). This indicated that Cu^{2+} removal occurred on the outer surface of Si-CHAP and it was probable for the formation of Cu precipitates. The pH dependence (Fig. 3 and Fig. 4) also suggested the possibility of precipitation. Sposito et al. [49] have shown that the coprecipitates of heavy metals are possible at long-term contacts. Li et al. [50] indicated that the compositions of calcium-deficient Na-containing carbonate hydroxyapatite modified with Cu^{2+} and Zn^{2+} displays a predominant dissolution-precipitation or coprecipitation mechanism and at the same time, adsorption and diffusion mechanism maybe also exist by means of ICP, XPS and FTIR.

In summary, the mechanisms involved in Cu^{2+} sorption by Si-CHAP may be divided into three parts (Fig. 12): 1) ion exchange followed by surface complexation; 2) Cu precipitation or co-precipitation and 3) electrostatic interactions between surface charge of Si-CHAP and copper ions in solutions.

3.9. Comparison of adsorption capacity with other adsorbents

The maximum monolayer adsorption capacities (Q_m) of Cu^{2+} onto the Si-CHAP was compared with the other adsorbents reported in previous studies and the values are shown in Table 4. Comparatively, Q_m values in this study are significantly higher (only with one exception) than the reported adsorbents (Table 4), suggesting that Si-CHAP is a potential adsorbent for removal Cu^{2+} from aqueous solutions.

4. Conclusions

In this study, Si-CHAP prepared from egg shell exhibited a high capacity for adsorption of Cu^{2+} from aqueous solution. The optimum pH value was 5.7 and the adsorption reached equilibrium at 90 min. Kinetics studies showed that the pseudo-second order model fitted better for the adsorption of Cu^{2+} bySi-CHAP. The sorption isotherms followed Langmuir model with a high adsorption capacity of 273.51 mg g^{-1} at 313 K. The thermodynamic studies showed that the adsorption of Cu^{2+} over Si-CHAP is an exothermic and spontaneous process. The results from IR, SEM and XRD showed that adsorption of Cu^{2+} led to changes in Si-CHAP, not only on the surface but also in the structure. The mechanism of Cu^{2+} adsorption on Si-CHAP included ion exchange, precipitation and electrostatic interactions. Furthermore, the well stability properties of the Si-CHAP adsorbent were confirmed through desorption assay. These results indicated that Si-CHAP may be an effective, alternative, low cost and environmentally friendly adsorbent for the rapid removal of $Cu^{2+}$from aqueous solutions.

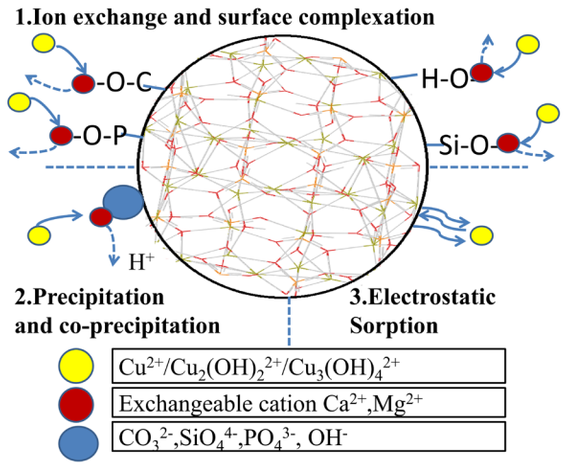

Fig. 12. The schematic illustration of Cu^{2+}adsorption mechanisms on Si-CHAP.

Acknowledgements

This study is supported by the Hunan Provincial Natural Science Foundation of China (No. 13JJ9018 and 2016JJ6013), the National Nature Science Foundation of China (No.21603065) and Research Center of Environmental Education, Key Research Base of Philosophy & Social Sciences in Hunan Province (HJ15k01).

References

[1] E.I. Solomon, D.E. Heppner, E.M. Johnston, J.W. Ginsbach, J. Cirera, M. Qayyum, M.T. Kieber-Emmons, C.H. Kjaergaard, R.G. Hadt, L. Tian, Copper active sites in biology, Chem. Rev., 114 (2014) 3659–3853.

[2] T. Mondol, J. Aden, P. Wittung-Stafshede, Copper binding triggers compaction in N-terminal tail of human copper pump ATP7B, Biochem. Bioph. Res. Co., 470 (2016) 663–669.

[3] F. Tisato, C. Marzano, M. Porchia, M. Pellei, C. Santini, Copper in diseases and treatments, and copper-based anticancer strategies, Med. Res. Rev., 30 (2010) 708–749.

[4] S.S. Stavitskaya, V.M. Vikarchuk, M.F. Kovtun, O.I. Poddubnaya, A.M. Puziy, Adsorption of copper ions by carbon adsorbents modified by phosphoric acid at different temperatures, J. Water Chem. Technol., 36 (2014) 110–114.

[5] (a) A.P. Mosier, J. Behnke, E.T. Jin, N.C. Cady, Microbial biofilms for the removal of Cu^{2+} from CMP wastewater, J. Environ. Manage., 160 (2015) 67–72. (b) O.N. Kononova, M.A. Kuznetsova, A.M. Mel'nikov, N.S. Karplyakova, Y.S. Kononov, Sorption recovery of copper(II) and zinc(II) from aqueous chloride solutions, J. Serb. Chem. Soc., 79 (2014) 1037–1049.

Table 4
Comparison of maximum adsorption capacity (Q_m) of Cu^{2+} with other adsorbents

Adsorbent	Q_m (mg g^{-1})	Isotherm	pH	Reference
N-HAP/chitosan (1537.6nm)	92.48	Langmuir	6	[51]
N-HAP/chitosan(47.6nm)	108.48	Langmuir	6	[51]
MgHAP/Fe_3O_4	305	Freundlich	5.9	[52]
Mg_2Al–LS–LDH*	71.4	Langmuir	5.7	[53]
XUS 43578	167.488	Langmuir	3	[9]
CR11	168.576	Langmuir	3	[9]
Coconut coir	71.1	Langmuir	7.0	[54]
Chitosan aerogel	35.05	Langmuir	–	[55]
Si-CHAP	273.52	Langmuir	5.7	This study

*LS: Sulfonated lignin, LDH: layered double hydroxides, Si-CHAP:Si-substituted carbonate hydroxyapatite, XUS 43578 and CR11: commercial chelating resins by Dow and Mitsubishi

[6] Y.H. Chou, J.H. Yu, Y.M. Liang, P.J. Wang, C.W. Li, S.S. Chen, Recovery of Cu(II) by chemical reduction using sodium dithionite, Chemosphere, 141 (2015) 183–188.
[7] G. Qiu, Q.Q. Xie, H.B. Liu, T.H. Chen, J.J. Xie, H.W. Li, Removal of Cu(II) from aqueous solutions using dolomite-palygorskite clay: Performance and mechanisms, Appl. Clay Sci., 118 (2015) 107–115.
[8] D.J. Ennigrou, M.B. Ali, M. Dhahbi, Copper and Zinc removal from aqueous solutions by polyacrylic acid assisted-ultrafiltration, Desalination, 343 (2014) 82–87.
[9] S. Edebali, E. Pehlivan, Evaluation of chelate and cation exchange resins to remove copper ions, Powder Technol., 301 (2016) 520–525.
[10] R. Najam, S.M.A. Andrabi, Removal of Cu(II), Zn(II) and Cd(II) ions from aqueous solutions by adsorption on walnut shell-Equilibrium and thermodynamic studies: treatment of effluents from electroplating industry, Desal. Water Treat., 57 (2016) 27363–27373.
[11] J.X. Li, B.Q. Jiang, Y. Liu, C.Q. Qiu, J.J. Hu, G.R. Qian, W.S. Guo, H.H. Ngo, Preparation and adsorption properties of magnetic chitosan composite adsorbent for Cu^{2+} removal, J. Clean. Prod., 158 (2017) 51–58.
[12] G.F. Coelho, A.C. GonCalves, J.C. Novoa-Munoz, D. Fernandez-Calvino, M. Arias-Estevez, M.J. Fernandez-Sanjurjo, E. Alvarez-Rodriguez, A. Nunez-Delgado, Competitive and non-competitive cadmium, copper and lead sorption/desorption on wheat straw affecting sustainability in vineyards, J. Clean. Prod., 139 (2016) 1496–1503.
[13] S.S.G. Santos, M.B.B. Pereira, R.K.S. Almeida, A.G. Souza, M.G. Fonseca, M. Jaber, Silylation of leached-vermiculites following reaction with imidazole and copper sorption behavior, J. Hazard. Mater., 306 (2016) 406–418.
[14] J. Pena, J.R. Bargar, G. Sposito, Copper sorption by the edge surfaces of synthetic birnessite nanoparticles, Chem. Geol., 396 (2015) 196–207.
[15] S. Parlayici, E. Pehlivan, Removal of metals by Fe_3O_4 loaded activated carbon prepared from plum stone (Prunus nigra): Kinetics and modelling study, Powder Technol., 317 (2017) 23–30.
[16] I. Mobasherpour, E. Salahi, M. Pazouki, Removal of divalent cadmium cations by means of synthetic nano crystallite hydroxyapatite, Desalination, 266 (2011) 142–148.
[17] W.I. Mortada, I.M.M. Kenawy, A.M. Abdelghany, A.M. Ismal, A.F. Donia, K.A. Nabieh, Determination of Cu^{2+}, Zn^{2+} and Pb^{2+} in biological and food samples by FAAS after preconcentration with hydroxyapatite nanorods originated from eggshell, Mat. Sci. Eng. C-Mater., 52 (2015) 288–296.
[18] S. Saber-Samandari, S. Saber-Samandari, N. Nezafati, K. Yahya, Efficient removal of lead (II) ions and methylene blue from aqueous solution using chitosan/Fe-hydroxyapatite nanocomposite beads, J. Environ. Manage., 146 (2014) 481–490.
[19] D.X. Liao, W. Zheng, X.M. Li, Q. Yang, X. Yue, L. Guo, G.M. Zeng, Removal of lead(II) from aqueous solutions using carbonate hydroxyapatite extracted from eggshell waste, J. Hazard. Mater., 177 (2010) 126–130.
[20] W.Q. Tang, R.Y. Zeng, Y.L. Feng, X.M. Li, W. Zhen, Removal of Cr(VI) from aqueous solution by nano-carbonate hydroxylapatite of different Ca/P molar ratios, Chem. Eng. J., 223 (2013) 340–346.
[21] L. Borum, O.C. Wilson, Surface modification of hydroxyapatite. Part II. Silica, Biomaterials, 24 (2003) 3681–3688.
[22] C. Zhang, L. Xiao, C. Liu, C. Duan, J. Yang, G.F. Wang, Ultrasonic chemistry fabrication of carbonated silicon-substituted hydroxyapatite nanopowder and its configuration representation, J. Chin. Ceram. Soc., 39 (2011) 1915–1921.
[23] C. Ding, D. Gong, P. Yu, J. Shao, M.E. Zhong, Removal of quinclorac herbicide from aqueous solution by chitosan/montmorillonite bionano composite, Desal. Water Treat., 57 (2016) 24970–24981
[24] M. Mohammadi, A. Ghaemi, M. Torab-Mostaedi, M. Asadollahzadeh, A. Hemmati, Adsorption of cadmium (II) and nickel (II) on dolomite powder, Desal. Water Treat., 53 (2015) 149–157.
[25] I. Langmuir, The adsorption of gases on plane surfaces of glass, mica and Platinum, J. Am. Chem. Soc., 40 (1918) 1361–1403.
[26] H. Freundlich, Udber die adsorption in Loesunger, Z. Physik. Chem., 57 (1907) 385–470.
[27] Y. Liu, Y.J. Liu, Biosorption isotherms, kinetics and thermodynamics, Sep. Purif. Technol., 61 (2008) 229–242.
[28] K.A. Hing, P.A. Revell, N. Smith, T. Buckland, Effect of silicon level on rate, quality and progression of bone healing within silicate-substituted porous hydroxyapatite scaffolds, Biomaterials, 27 (2006) 5014–5026.
[29] L. Borum-Nicholas, O.C. Wilson, Surface modification of hydroxyapatite. Part I. Dodecyl alcohol, Biomaterials, 24 (2003) 3671–3679.
[30] X.L. Tang, X.F. Xiao, R.F. Liu, Structural characterization of silicon-substituted hydroxyapatite synthesized by a hydrothermal method, Mater. Lett., 59 (2005) 3841–3846.
[31] E. Zhang, C.M. Zou, G.N. Yu, Surface microstructure and cell biocompatibility of silicon-substituted hydroxyapatite coating on titanium substrate prepared by a biomimetic process, Mat. Sci. Eng. C-Bio. S., 29 (2009) 298–305.
[32] W.T. Tsai, J.M. Yang, C.W. Lai, Y.H. Cheng, C.C. Lin, C.W. Yeh, Characterization and adsorption properties of eggshells and eggshell membrane, Biores. Technol., 97 (2006) 488–493.
[33] J. Su, H.G. Huang, X.Y. Jin, X.Q. Lu, Z.L. Chen, Synthesis, characterization and kinetic of a surfactant-modified bentonite used to remove As(III) and As(V) from aqueous solution, J. Hazard. Mater., 185 (2011) 63–70.
[34] G. Chen, K.J. Shah, L.Shi, P.C. Chiang, Removal of Cd(II) and Pb(II) ions from aqueous solutions by synthetic mineral adsorbent: Performance and mechanisms, Appl. Surf. Sci., 409 (2017) 296–305.
[35] M. Ghasemi, M. Naushad, N. Ghasemi, Y. Khosravi-Fard, Adsorption of Pb(II) from aqueous solution using new adsorbents prepared from agricultural waste: Adsorption isotherm and kinetic studies, J. Ind. Eng. Chem., 20 (2014) 2193–2199.
[36] C. Appel, L.Q. Ma, R.D. Rhue, E. Kennelley, Point of zero charge detemination in soils and minerals via traditional methods and detection of electroacoustic mobility, Geoderma, 113 (2003) 77–93.
[37] S. Saber-Samandari, S. Saber-Samandari, M. Gazi, Cellulose-graft-polyacrylamide/hydroxyapatite composite hydrogel with possible application in removal of Cu (II) ions, React. Funct. Polym., 73 (2013) 1523–1530.
[38] A. Dabrowski, P. Podkoscielny, Z. Hubicki, M. Barczak, Adsorption of phenolic compounds by activated carbon - a critical review, Chemosphere, 58 (2005) 1049–1070.
[39] H. Ge, J. Wang, Ear-like poly (acrylic acid)-activated carbon nanocomposite: A highly efficient adsorbent for removal of Cd(II) from aqueous solutions, Chemosphere, 169 (2017) 443–449.
[40] G. Yang, L. Tang, X. Lei, G. Zeng, Y. Cai, X. Wei, Y. Zhou, S. Li, Y. Fang, Y. Zhang, Cd(II) removal from aqueous solution by adsorption on α-ketoglutaric acid-modified magnetic chitosan, Appl. Surf. Sci., 292 (2014) 710–716.
[41] L. Seid , D. Chouder, N. Maouche, I. Bakas, N. Barka, Removal of Cd(II) and Co(II) ions from aqueous solutions by polypyrrole particles: Kinetics, equilibrium and thermodynamics, J. Taiwan Inst. Chem. E., 45 (2014) 2969–2974.
[42] Z. Elouear, J. Bouzid, N. Boujelben, M. Feki, F. Jamoussi, A. Montiel, Heavy metal removal from aqueous solutions by activated phosphate rock, J. Hazard. Mater., 156 (2008) 412–420.
[43] S. Sugiyama, H. Matsumoto, T. Ichii, H. Hayashi, Y. Hiraga, N. Shigemoto, Enhancement of lead-barium exchangeability of barium hydroxyapatite, J. Colloid. Interf. Sci., 238 (2001) 183–187.
[44] S. Meski, S. Ziani, H. Khireddine, Removal of lead ions by hydroxyapatite prepared from the egg shell, J. Chem. Eng. Data, 55 (2010) 3923–3928.
[45] Y.J. Lin, M.S. Wang, C.J. Liu, H.J. Huang, Defects, stress and abnormal shift of the (0 0 2) diffraction peak for Li-doped ZnO films, Appl. Surf. Sci., 256 (2010) 7623–7627.
[46] S. Shanmugam, B. Gopal, Copper substituted hydroxyapatite and fluorapatite: Synthesis, characterization and antimicrobial properties, Ceram. Int., 40 (2014) 15655–15662.

[47] T. Ishikawa, M. Wakamura, S. Kondo, Surface characterization of calcium hydroxylapatite by Fourier transform infrared spectroscopy, Langmuir, 5 (1989) 140–144.
[48] S. Hokkanen, A. Bhatnagar, E. Repo, S. Lou, M. Sillanpaa, Calcium hydroxyapatite microfibrillated cellulose composite as a potential adsorbent for the removal of Cr(VI) from aqueous solution, Chem. Eng. J., 283 (2016) 445–452.
[49] G. Sposito, Distinguishing adsorption from surface precipitation, ACS Publications, 1986.
[50] J.D. Li, Y.B. Li, L. Zhang, Y. Zuo, Composition of calcium deficient Na-containing carbonate hydroxyapatite modified with Cu(II) and Zn(II) ions, Appl. Surf. Sci., 254 (2008) 2844–2850.
[51] R. Bazargan-Lari, H.R. Zafarani, M.E. Bahrololoom, A. Nemati, Removal of Cu(II) ions from aqueous solutions by low-cost natural hydroxyapatite/chitosan composite: Equilibrium, kinetic and thermodynamic studies, J. Taiwan Inst. Chem. E., 45 (2014) 1642–1648.
[52] L.M. Cui, L.H. Hu, X.Y. Guo, Y.K. Zhang, Y.G. Wang, Q. Wei, B. Du, Kinetic, isotherm and thermodynamic investigations of Cu^{2+} adsorption onto magnesium hydroxyapatite/ferroferric oxide nano-composites with easy magnetic separation assistance, J. Mol. Liq., 198 (2014) 157–163.
[53] G. Huang, D. Wang, S. Ma, J. Chen, L. Jiang, P. Wang, A new, low-cost adsorbent: preparation, characterization, and adsorption behavior of Pb (II) and Cu (II), J. Colloid. Interf. Sci., 445 (2015) 294–302.
[54] N.B. Chang, C. Houmann, K.S. Lin, M. Wanielista, Fate and transport with material response characterization of green sorption media for copper removal via adsorption process, Chemosphere, 144 (2016) 1280–1289.
[55] A. Li, R. Lin, C. Lin, B. He, T. Zheng, L. Lu, Y. Cao, An environment-friendly and multi-functional absorbent from chitosan for organic pollutants and heavy metal ion, Carbohyd. Polym., 148 (2016) 272–280.